Title
A catchment scale water balance model for FIFE

Journal
Journal of Geophysical Research, 97(D17)

ISSN
0148-0227

Authors
Famiglietti, J. S
Wood, E. F
Sivapalan, M.
et al.

Publication Date
1992

DOI
10.1029/92JD01049

Peer reviewed

JOURNAL OF GEOPHYSICAL RESEARCH, VOL. 97, NO. D17, PAGES 18,997–19,007, NOVEMBER 30, 1992

A Catchment Scale Water Balance Model for FIFE

J. S. FAMIGLIETTI AND E. F. WOOD

Water Resources Program, Department of Civil Engineering and Operations Research, Princeton University, Princeton, New Jersey

M. SIVAPALAN

Centre for Water Research, The University of Western Australia, Nedlands

D. J. THONGS

Water Resources Program, Department of Civil Engineering and Operations Research, Princeton University, Princeton, New Jersey

A catchment scale water balance model is presented and used to predict evaporation from the King's Creek catchment at the First ISLSCP Field Experiment site on the Konza Prairie, Kansas. The model incorporates spatial variability in topography, soils, and precipitation to compute the land surface hydrologic fluxes. A network of 20 rain gages was employed to measure rainfall across the catchment in the summer of 1987. These data were spatially interpolated and used to drive the model during storm periods. During interstorm periods the model was driven by the estimated potential evaporation, which was calculated using net radiation data collected at site 2. Model-computed evaporation is compared to that observed, both at site 2 (grid location 1916-BRS) and the catchment scale, for the simulation period from June 1 to October 9, 1987.

INTRODUCTION

One of the objectives of the International Satellite Land Surface Climatology Project (ISLSCP) is the development of methods for deriving quantitative information on land surface-atmospheric interactions. Central to these interactions are the dynamics of the hydrologic balance at large scales and the role that spatial heterogeneity (of land surface properties and processes) plays in these dynamics. During the First ISLSCP Field Experiment (FIFE), various components of the water balance were observed over a 15-km by 15-km region, either directly or remotely. Consequently, the FIFE data set is unique in that it is a relatively large scale data base in which subgrid scale variability in certain processes (for example, rainfall and evapotranspiration) or properties (for example, soil type) is well documented. FIFE comes at a critical time in that hydrologists are giving considerable attention to the issues of spatial variability, and climatologists are addressing the issues of modeling land surface-atmospheric interactions at scales relevant to general circulation models (GCMs). At the GCM grid scales, considerable subgrid spatial variability exists that influences grid scale fluxes. The form of such macroscale water balance models, which preserve subgrid variability, is the ultimate objective of this research.

This paper represents a first step toward that goal. Here we present a simplified, distributed version of a macroscale land surface hydrology model that includes spatial variability in topography, soils, and rainfall, with simple couplings to the atmosphere. This study extends previous work by *Sivapalan et al.* [1987] by including interstorm evaporation processes. The model is presented in spatially distributed form to facilitate comparison with the FIFE data set. Water balance data, including precipitation, evaporation, streamflow, and surface soil moisture, are available for the King's Creek catchment in the northwestern quadrant of the FIFE site (see Figure 1): therefore we will begin our modeling studies at the catchment scale. Catchment topography is represented by a 30-m digital elevation model (DEM). Soil properties and other pertinent land surface information are overlaid on a corresponding geographic information system (GIS). Model inputs can therefore be spatially distributed, and the resulting spatial variations in model outputs, which represent the dynamics of land surface-atmosphere interactions, can be observed in three dimensions. A statistical-dynamical version of this model, more appropriate for use in GCMs, is presented by *Famiglietti and Wood* [1991*a*].

In the model version presented here, the link between the spatial variability in land surface properties and the resulting spatial variability in hydrologic fluxes is emphasized. Flow in the unsaturated zone is simplified in an attempt to understand some basic principles of land surface-atmosphere interactions. Current research is aimed at improving the modeled unsaturated zone physics and energy balance components, as well as thorough testing of the model with the FIFE data set. In this paper, however, we wish to present the simplified model formulation and results for interstorm evaporation.

Paper number 92JD01049.
0148-0227/92/92JD-01049$05.00

WATER BALANCE MODEL

FIFE efforts toward identification of the land surface energy fluxes would benefit from the independent estimation of areal and temporal evaporation that a terrestrial water balance could provide. The water balance for a catchment for a period Δt can be expressed as

$$E = P - Q_s - Q_g - \Delta S_u - \Delta S_g - \Delta S_s, \qquad (1)$$

in which each term is an equivalent volume of liquid water and E represents evaporation; P, precipitation; Q_s, stream-

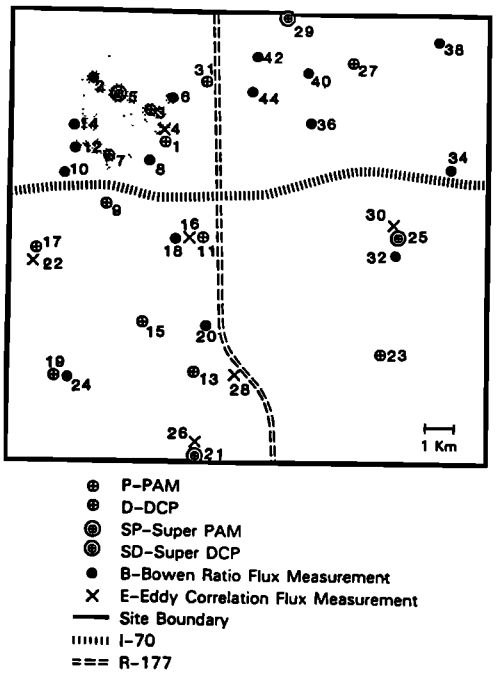

Fig. 1. FIFE site showing approximate locations of King's Creek catchment (shaded area), flux stations, and meteorological stations. Portable automated mesonet meteorological stations are abbreviated PAM. U.S. Army Corps of Engineers Data Control Platform meteorological stations are abbreviated DCP.

flow out of the catchment; Q_g, groundwater discharge out of the catchment; ΔS_u, change in storage in the unsaturated zone; ΔS_g, change in groundwater storage; and ΔS_s, change of storage in surface water bodies. Of the six terms on the right-hand side of (1) we will ignore the terms Q_g and ΔS_s. Because the watershed system at King's Creek consists of thin soils overlying impermeable bedrock, we will ignore any potential groundwater runoff from deeper aquifers that is not intercepted by the channel system. Changes in surface water storage can also be ignored owing to the lack of open water bodies. The change in groundwater storage, ΔS_g, represents the change in storage of a saturated layer of soil overlying bedrock. Its estimation is discussed later. Since evaporation implicitly depends on the remaining terms on the right-hand side of (1), P, Q_s, ΔS_u, and ΔS_g, it is important to estimate these terms accurately. In the sections that follow, we describe how the various components in (1) are measured or physically modeled.

Precipitation

It is important to estimate rainfall volumes from individual storms accurately so that the water balance calculations are not in error. Prior to FIFE a network design analysis based on estimating individual storm volumes was carried out. This analysis indicated that approximately 20 gages within the King's Creek watershed would provide an estimate of storm volumes to within 15%.

Twenty tipping bucket rain gages, which recorded 0.20 mm tipping times on a data logger, were used to measure the rainfall across the catchment. The data were downloaded in the field with a portable personal computer. Catchment scale rainfall fields were estimated by interpolating over the watershed using a kriging algorithm and a theoretical spatial correlation function [*Sivapalan and Wood*, 1987]. Figure 2 gives the daily basin average precipitation from June 1 to October 15, 1987.

Streamflow Generation and Evaporation

Land surface hydrologic fluxes and spatial variability. The spatial distribution of local catchment characteristics such as topography, soil type, soil moisture, and vegetation plays a major role in the partitioning of precipitation into runoff and infiltrated water. Rain falling on the saturated areas near stream networks becomes runoff, which is often referred to as saturation excess runoff. At some unsaturated locations in the catchment, local soil properties combine in such a way that the local capacity to transmit water to the subsurface is limited and, depending on local rainfall intensity, may be less than the local rate of precipitation. In this case, some fraction of rain falling on these areas infiltrates into the soil, whereas the remainder flows as infiltration excess runoff, often to the stream network. At other unsaturated locations the local capacity to infiltrate water is such that all the incident rainfall can be transmitted to the subsurface. These areas remain unsaturated during rain events.

During interstorm periods an analogous scenario exists, in which the now upward flux of evapotranspiration depends on the spatial distribution of surface soil moisture and soil properties. Saturated areas in the catchment will evaporate or transpire at the potential rate, which is a function of atmospheric conditions. Other locations will exist in the catchment that are not saturated, but whose soil parameters act in concert, so that for the particular level of atmospheric forcing the local upward transmission rate can still meet the evaporative demands of the atmosphere. Finally, there remains a portion of the catchment surface that owing to local soil and climatic conditions can only evaporate or transpire at a rate that is less than the atmospheric demand for water vapor. These areas contribute moisture to the atmosphere at their own soil-controlled or vegetation-controlled rates.

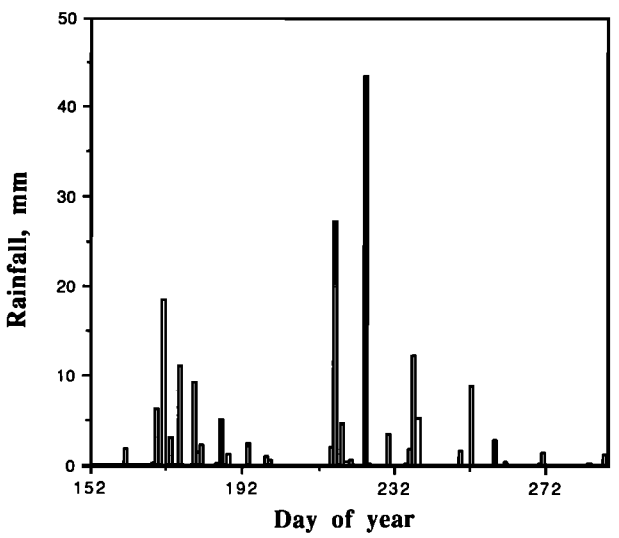

Fig. 2. Daily basin average precipitation from June 1 to October 15, 1987.

Recent field studies into hydrologic responses have led to increased recognition that subsurface flows play a very important role in the redistribution of soil moisture between storm events. For areas of relatively shallow soil the local topography exerts a dominant control on these subsurface flows. In particular, areas of higher antecedent wetness, which have a greater likelihood of generating runoff and evaporation at the potential rate, should be expected in areas of convergent flow in plan and concave slopes in profile. These areas are commonly found in hillslope hollows and above the heads of the smallest (first order) stream channels. Similarly, the variability in soil properties such as saturated hydraulic conductivity and soil texture greatly influences the vertical and lateral transmission properties of hillslopes.

We now present a formulation for the spatial distribution of saturated land surface, making use of information on the variability of topography and soil characteristics. To this soil moisture component we will couple our equations for the land surface hydrologic fluxes of evaporation, infiltration and saturation excess runoff, and base flow. These flux equations will be parameterized in terms of intrinsic soil properties and surface soil moisture, so that local fluxes will depend on local conditions and the total of a particular flux over the land surface will be a sum over the spatially varying conditions on the catchment.

Spatial-temporal dynamics of saturated land surface areas. The starting point for the water balance model is the runoff generation model of *Sivapalan et al.* [1987]. Portions of that work are briefly summarized here for the convenience of the reader. Their model starts from the premise that at depth the water table is recharged at a steady rate r, so that at any location i the downslope saturated flow q_i is given by

$$q_i = ar, \tag{2}$$

where a is the upslope contributing area that drains through the unit contour at i. The water table is assumed to be nearly parallel to the soil surface, so that the local hydraulic gradient is close to the local slope angle, tan β, and the saturated hydraulic conductivity is assumed to decline exponentially with depth [*Beven*, 1982]. Then the downslope saturated flow is shown to also equal

$$q_i = T_i \exp(-fz_{w_i}) \tan \beta, \tag{3}$$

where T_i is the local saturated transmissivity (approximately equal to the local surface saturated hydraulic conductivity divided by f), f is a parameter related to the decay of saturated hydraulic conductivity with depth, and z_{w_i} is the local water table depth (positive downward). If the subsurface hydrologic response is assumed to proceed as a series of quasi-steady states, (2) and (3) can be equated. Integrating over the catchment area to obtain a catchment average depth to water table, it can be shown after some algebra that the relationship between this average depth $\bar{z}$ and a local depth z_{w_i} is given by

$$z_{w_i} - \bar{z} = \frac{1}{f}\left\{\Lambda - \ln\left(\frac{aT_e}{T_i \tan \beta}\right)\right\}, \tag{4}$$

where ln (T_e) is the areal average value of ln (T_i) across the catchment and Λ is the expected value of the topographic variable ln $(a/\tan \beta)$ which is a constant for a particular catchment. Equation (4) implies that all locations in the catchment having the same value of the combined topographic-soil index ln $\{(aT_e)/(T_i \tan \beta)\}$ will have the same relationship between local depth to water table and mean depth, that is, it is an index of local hydrologic similarity. Inspection of (4) shows that locations with high values of the topographic-soil index relative to the catchment average, Λ, will have smaller water table depths and will consequently have a greater propensity to saturate the surface.

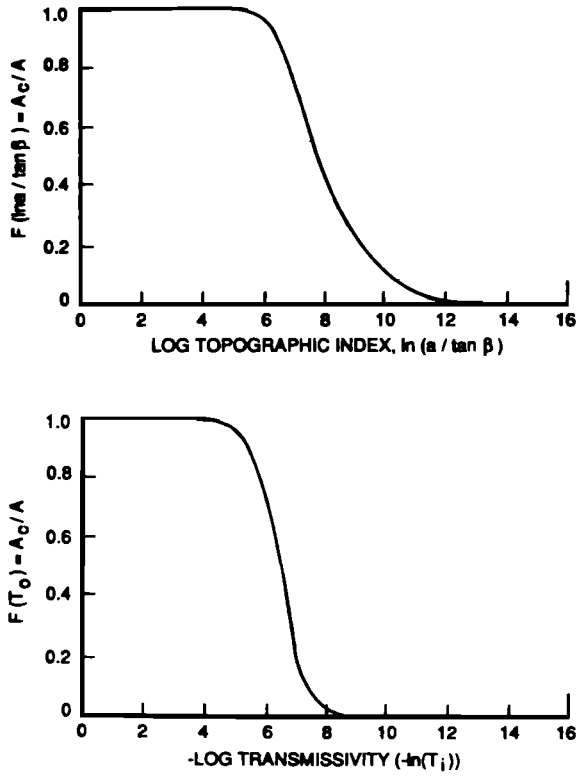

Fig. 3. (Top) Cumulative distribution of log topographic index for King's Creek catchment. (Bottom) Cumulative distribution of log transmissivity for King's Creek catchment.

In fact, for any particular value of $\bar{z}$, knowledge of the pattern of soil and topography (the topographic-soil index) allows prediction of those areas where $z_{w_i} \leq 0$ and therefore the saturated contributing area. More strictly, *Sivapalan et al.* [1987] define the area of saturation where $z_{w_i} \leq \psi_B$ and ψ_B is the depth of the capillary fringe. Prediction of the changes through time in $\bar{z}$ then allows the dynamic expansion and contraction of this contributing area to be modeled.

We may separate the topographic and soil contributions to the combined index by rewriting (4) as

$$f(z_{w_i} - \bar{z}) = -\{\ln(a/\tan \beta) - \Lambda\} + \{\ln(T_i) - \ln(T_e)\}. \tag{5}$$

The variations of the topographic variable $(a/\tan \beta)$ and the soil transmissivity T_i over the catchment may both be represented as distribution functions. Figure 3 shows the cumulative distribution functions of the topographic index, $F\{\ln(a/\tan \beta)\}$, and the transmissivity, $F\{\ln(T_i)\}$, for the King's Creek catchment. The right-hand side of (5) is then clearly the sum of two deviations of the local values of ln $(a/\tan \beta)$ and T_i from their catchment mean values, whereas the left-hand side of (5) represents the local deviation in water table depth from the catchment mean value scaled by the parameter f. Figure 3 shows that the variability

in the topographic index is far greater than the variability in transmissivity. Thus variability in the transmissivity will have a relatively smaller effect on the distribution of the combined topographic-soil index and consequently on predicted patterns of local water table depths and saturated contributing areas.

Given the model for water table dynamics, the surface soil moisture can be inferred from the water table depth by means of some simplifying assumptions. Saturated areas have a surface soil moisture equal to the saturation value of moisture content for the particular soil type. The surface soil moisture of unsaturated areas is assumed uniform with depth to the water table. Research efforts are currently directed toward the improvement of these simplified unsaturated zone physics in the model.

Saturation excess runoff. As described earlier, saturation excess runoff occurs when rain falls directly on the saturated areas adjacent to the stream network. Again, these are the areas where $z_{w_i} \leq \psi_B$, or

$$\ln \{(aT_e)/(T_i \tan \beta)\} \geq f(\bar{z} - \psi_B) + \Lambda. \quad (6)$$

Additionally, there are those unsaturated areas in the catchment that have a small storage deficit that can easily be satisfied and become saturated during a storm. Further contributions to saturation excess runoff are made by this mechanism.

Infiltration excess runoff. The governing equation for soil water flow in the unsaturated zone is given by *Richards* [1931] as

$$\frac{\partial \theta}{\partial t} = \frac{\partial}{\partial z}\left[K(\psi)\frac{\partial \psi}{\partial z} + K(\psi)\right], \quad (7)$$

where θ is the moisture content, ψ is the matric head, and K is the hydraulic conductivity. As is well known, the solution of (7) is not easy, owing to the highly nonlinear nature of $K(\psi)$, the hysteresis during wetting and drying cycles, and the boundary conditions encountered in nature.

Philip [1957] solved (7) with the simplified boundary conditions of an initially uniform moisture profile in the unsaturated zone and a step change in soil moisture at the soil surface:

$$\theta = \theta_i \qquad t = 0 \qquad z \geq 0 \quad (8a)$$

$$\theta = \theta_0 \qquad t > 0 \qquad z = 0, \quad (8b)$$

where θ_i is the initial moisture content and θ_0 is the value of soil moisture at the surface during precipitation. His simplified infiltration equation is given by

$$d_I^* = \tfrac{1}{2} s t^{-1/2} + cK_S, \quad (9)$$

where d_I^* is the infiltration capacity, s is the sorptivity, K_S is the saturated hydraulic conductivity, and cK_S includes the effect of gravity.

For the case of variable rainfall we apply the time condensation approximation (TCA) [*Sherman*, 1943; *Ibrahim and Brutsaert*, 1968; *Reeves and Miller*, 1975; *Milly*, 1986]. The idea behind the TCA is to correct the infiltration equation, which was derived from boundary conditions of immediate ponding. In reality, ponding rarely, if ever, occurs immediately, and rainfall at a point varies in intensity over time. Thus the infiltration capacity predicted by (9) for real rainfall would be too small. One way to extend the simplified Philip's equation is to remove time from (9) by making d_I^* a function of the cumulative infiltration, D_I [*Milly*, 1986]. Integrating (9) and substituting for time, $d_I^*(D_I)$ is

$$d_I^*(D_I) = cK_S\left\{1 + \left[\left(1 + \frac{4cK_S D_I}{s^2}\right)^{1/2} - 1\right]^{-1}\right\}. \quad (10)$$

Then, at any time, the local actual infiltration rate, d_{I_i}, is given by

$$d_{I_i} = \min [d_{I_i}^*(D_{I_i}), p_i], \quad (11)$$

where p_i is the precipitation rate. Infiltration excess runoff is generated on those parts of the catchment where $p_i > d_{I_i}^*$.

From (10) it is clear that the infiltration capacity is a function of both the saturated hydraulic conductivity and the sorptivity. Saturated hydraulic conductivity varies spatially in the model. The sorptivity expression utilized here is given by *Sivapalan et al.* [1987] and is a function of the spatially variable soil texture parameters as well as soil moisture in the unsaturated zone. Therefore the model should simulate the spatial variability in infiltration reasonably well.

Subsurface flow. The contribution of the catchment to runoff by subsurface flow, Q_b, is given by integrating the downslope saturated flow, q_i, along both sides of the stream network, so that

$$Q_{bs} = Q_0 \exp(-f\bar{z})\Delta t, \quad (12)$$

where [*Sivapalan et al.*, 1987]

$$Q_0 = AT_e \exp(-\Lambda), \quad (13)$$

and A is the catchment area. Again, this is the subsurface flow exiting the hillslope at the stream channel. Note that the quasi-steady state approach implicitly incorporates the dynamics of subsurface flow on hillslopes during storms; as $\bar{z}$ is updated, the water table profile shifts in response and Q_{bs} increases.

The catchment scale flux of surface runoff. The total streamflow volume for the catchment is obtained by summing the contribution to surface runoff from each grid square in the model. Additional contributions to streamflow come from the subsurface flow term Q_{bs}. During any time step, the total streamflow volume Q_s is given by

$$Q_s = Q_{se} + Q_{ie} + Q_{bs}, \quad (14)$$

where Q_{se} is the volume of saturation excess runoff generated in the catchment and Q_{ie} is the volume of infiltration excess runoff. The volume of saturation excess runoff is given by

$$Q_{se} = \Delta A \sum_{i \in \mathcal{S}} p_i \Delta t + \Delta A \sum_{i \in \mathcal{U}} (p_i \Delta t - S_i), \quad (15)$$

where ΔA is the incremental area representing the location i; $\mathcal{S}$ is the set of saturated locations, that is, where $z_{w_i} \leq \psi_{B_i}$; z_{w_i} is the local water table depth; ψ_{B_i} is the local capillary fringe height; p_i is the incident rainfall rate on the grid square during a time step Δt; $\mathcal{U}$ is the set of all unsaturated locations, where $S_i < p_i \Delta t < d_{I_i}^* \Delta t$; and S_i is the local storage deficit. The magnitude of S_i is a function of water table depth z_{w_i}, where $S_i = (\theta_{s_i} - \theta_i)(z_{w_i} - \psi_{B_i})$. The catchment volume of infiltration excess runoff is given by

$$Q_{ie} = \Delta A \sum_{i \varepsilon \nu} (p_i - d_{I_i}^*)\Delta t, \tag{16}$$

where ν is the set of all unsaturated locations where $p_i > d_{I_i}^*$ and $d_{I_i}^*$ is the local infiltration capacity.

Evaporation. The present section applies to evaporation from unsaturated locations. Saturated locations are allowed to evaporate at the potential rate in the model. Note that there is no explicit treatment of vegetation in this paper. The inclusion of vegetation in the model is coincident with ongoing research to improve the simulation of unsaturated zone processes.

Under constant atmospheric demand, two stages have been recognized in the unsteady drying of a soil profile [*Brutsaert*, 1982; *Hillel*, 1980]. In the first stage, the moist soil profile can fully supply all the water demanded by the atmosphere. This stage is known as the atmosphere-controlled stage. Evaporation proceeds at the potential rate, which is dictated by external climatic conditions. The duration of this stage depends on the rate of atmospheric demand and the ability of the soil to supply moisture at this rate. *Hillel* [1980] notes that this stage is frequently brief and usually ceases within a few days.

As the soil near the surface dries out, moisture can no longer be delivered at the rate demanded by the atmosphere. Instead, the moisture delivery rate is limited by the properties of the soil profile. Thus this stage of soil drying is known as the soil-controlled or falling rate stage. *Brutsaert* [1982] notes that at any one point, the transition from soil to atmosphere control is rapid, but over the entire catchment the changeover will be gradual.

The governing equation for the soil-controlled stage of evaporation is obtained by combining soil water continuity with Darcy's law, which yields

$$\frac{\partial \theta}{\partial t} = \frac{\partial}{\partial z}\left[K(\psi)\frac{\partial \psi}{\partial z} - K(\psi)\right]. \tag{17}$$

Like (7), the solution of (17) is complicated by nonlinearities and hysteresis.

A simplified formulation considers the soil-controlled stage as a desorption problem only. Neglecting gravity, (17) becomes

$$\frac{\partial \theta}{\partial t} = \frac{\partial}{\partial z}\left[K(\psi)\frac{\partial \psi}{\partial z}\right]. \tag{18}$$

For the simplified boundary conditions

$$\theta = \theta_i \qquad t = 0 \qquad z \geq 0 \tag{19a}$$

$$\theta = \theta_d \qquad t > 0 \qquad z = 0, \tag{19b}$$

where θ_d is the moisture at the dry soil surface. Equation (18) can be reduced to an ordinary differential equation, and the evaporation capacity, d_e^*, is given by

$$d_e^* = \tfrac{1}{2} s_e t^{-1/2}, \tag{20}$$

where s_e is the desorptivity which is dependent on soil type, θ_d, and θ_i.

Applying time condensation again, (20) becomes

$$d_e^*(D_e) = \frac{s_e^2}{2D_e}, \tag{21}$$

where D_e is the cumulative evaporation. To account for diurnal variation in the atmospheric demand for water vapor, at any time during the interstorm period, the actual evaporation rate at any point, d_{e_i}, can now be expressed as

$$d_{e_i} = \min\,[d_{e_i}^*(D_{e_i}),\ e_{pe}], \tag{22}$$

where e_{pe} is the potential rate of evaporation, which is assumed to be known or obtained from atmospheric variables.

In (20) the desorptivity varies with soil moisture content and other parameters dependent on soil type. As in the infiltration case, the actual rate of evaporation is then a function of soil type, soil moisture, and atmospheric forcing. Since soil property parameters vary spatially, different unsaturated locations in the catchment can evaporate at different rates, depending on local land surface and climate conditions.

The catchment scale flux of evaporation. The total flux of evaporation from the catchment is obtained by summing the contributions from each grid square in the model. During any time step, the total volume of evaporation, E, is given by

$$E = E_{s_{pe}} + E_{u_{pe}} + E_{u_{sc}}, \tag{23}$$

where $E_{s_{pe}}$ represents the contribution from saturated areas evaporating at the potential rate, $E_{u_{pe}}$ represents the contribution from unsaturated areas evaporating at the potential rate, and $E_{u_{sc}}$ represents the contribution from locations that evaporate at local soil controlled rates. The volume of evaporation from saturated areas is given by

$$E_{s_{pe}} = \Delta A \sum_{i \varepsilon \mathcal{S}} e_{pe}\Delta t, \tag{24}$$

where $\mathcal{S}$ is the set of saturated locations for the time step. The volume of evaporation contributed by unsaturated areas at the potential rate is given by

$$E_{u_{pe}} = \Delta A \sum_{i \varepsilon \mathcal{W}} e_{pe}\Delta t, \tag{25}$$

where $\mathcal{W}$ is the set of unsaturated locations with $e_{pe} \leq d_{e_i}^*$ and $d_{e_i}^*$ is the local evaporation capacity. The volume of evaporation contributed by unsaturated locations at their local soil controlled rates is given by

$$E_{u_{sc}} = \Delta A \sum_{i \varepsilon \mathcal{X}} d_{e_i}^* \Delta t, \tag{26}$$

where $\mathcal{X}$ is the set of unsaturated locations where $d_{e_i}^* < e_{pe}$.

Storage in the Unsaturated and Saturated Zones

During a storm period, infiltrated water accumulates in grid square storage deficits, where local deficit magnitude is a function of water table depth. The sum of this infiltrated water over the catchment constitutes ΔS_u, the catchment-wide change in unsaturated zone storage for the time step. This change in unsaturated zone storage is given by

$$\Delta S_u = \Delta A \sum_{i \varepsilon \mathcal{U}^*} \min\,(d_{I_i}^*,\ p_i)\Delta t, \tag{27}$$

where $\mathcal{U}^*$ is the set of all unsaturated locations. At the end of a storm event, water stored in the unsaturated zone is allowed to drain to the water table. This downward flux,

TABLE 1. Soil Types and Properties

Soil Type	Parameter Value						
	K_s, m h^{-1}	f, m^{-1}	θ_s	θ_r	ψ_B, m	B	Cover, %
Alluvial land	0.018	1.51	0.49	0.04	0.27	0.18	0.08
Benfield-Florence complex	0.019	3.74	0.47	0.06	0.33	0.14	0.52
Clime-Sogn complex	0.019	5.17	0.47	0.04	0.33	0.15	0.30
Dwight-Irwin complex	0.016	2.22	0.48	0.05	0.33	0.14	0.04
Irwin silty clay loam	0.033	2.11	0.48	0.05	0.34	0.13	0.01
Irwin silty clay loam (eroded)	0.010	2.11	0.48	0.05	0.34	0.13	0.01
Ivan and Kennebec silt loams	0.033	2.18	0.48	0.04	0.30	0.16	0.01
Reading silt loam	0.033	2.18	0.48	0.04	0.30	0.16	0.01
Stony steep land	0.010	4.91	0.47	0.04	0.33	0.15	0.01
Tully silty clay loam	0.010	2.35	0.48	0.05	0.34	0.13	0.01

corrected for losses to base flow, becomes ΔS_g, or the change in saturated storage for the catchment. The change in saturated storage is updated at the end of each storm event and for each time step in the interstorm period. At the end of a storm, ΔS_g is given by

$$\Delta S_g = \Delta A \sum_{i \varepsilon \mathcal{U}^*} D_{I_i} - Q_{b_s}, \tag{28}$$

where D_{I_i} is the cumulative infiltration for a grid square for the storm and Q_{b_s} is the storm volume of base flow. This procedure is the equivalent of updating the average water table depth, $\bar{z}$, in (4), which is discussed later.

During interstorm periods the soil moisture profiles in individual unsaturated locations are maintained at their prescribed levels which is the equivalent of maintaining the soil moisture profiles at their field capacity. Evaporated water must then be supplied by the water table, so that ΔS_g is comprised of evaporative losses and catchment drainage due to base flow. The change in saturated storage is given by

$$\Delta S_g = -\left(\Delta A \sum_{i \varepsilon \mathcal{U}^*} \min (d^*_{e_i}, e_{pe}) \Delta t + \Delta A \sum_{i \varepsilon \mathcal{S}} e_{pe} \Delta t + Q_{bs} \right) \tag{29}$$

for each interstorm time step.

Data

Topography. Catchment topography is represented by a 30-m U.S. Geological Survey DEM. From the DEM the contributing area, a, and the local slope, β, can be computed. From these two variables the topographic index, ln (a/tan β), can be determined for each model grid square.

Soils. The soil types for each grid square on the catchment have been coregistered in a GIS. For each of the soil types in the catchment, soil texture classifications are available from the local U.S. Department of Agriculture Soil Conservation Service soil survey [*Jantz et al.*, 1975]. Representative profiles for each soil type are described. This information includes the areal variation in soil texture within each soil type, the variation in saturated hydraulic conductivity with depth, and depth to bedrock. From this information a weighted average value of the saturated hydraulic conductivity and the parameter f were determined for each soil type (although a catchment average value of f is used in equations (4) and (12)). Given this information, the local value of transmissivity, T_i, can be calculated and its areal average, T_e, can be computed. Combining this information with the topographic information given previously yields ln $\{(aT_e)/(T_i \tan \beta)\}$, the combined topography-soils index, for each grid square.

Other soil textural parameters are required for the local calculation of sorptivity and desorptivity. These are the *Brooks and Corey* [1964] parameters that describe the saturation moisture content, θ_s, the residual moisture content, θ_r, the pore size distribution index, B, and the bubbling pressure, ψ_B. Average values of these parameters for each soil texture are given by *Rawls et al.* [1982]. From this information, weighted averages of θ_s, θ_r, B, and ψ_B were calculated for each soil type and thus each grid square in the catchment. This information is presented in Table 1 for each soil type in the King's Creek catchment.

Climate. Precipitation data are described in a previous section. These data are used to force the storm components of the model. The flux of latent heat and associated energy balance data were collected at the various flux stations at the FIFE site. This information is available through the FIFE information system and is used to drive the interstorm components of the model, as well as for comparison of modeled latent heat fluxes to those observed.

Parameter Estimation

Most of the model parameters are based on soil or topographic information; their measurement or estimation has been described above. However, the estimation of the parameters Q_0 and f has been handled in alternative ways by various researchers. As described above, they can be determined from DEM and soil survey data. They can also be obtained from field and map information [*Beven and Kirkby*, 1979; *Beven et al.*, 1984]. Calibration to a number of recession curves was the method proposed by *Beven and Wood* [1983]. *Famiglietti and Wood* [1991*b*] presented a technique for the estimation of the two parameters using remotely sensed microwave soil moisture data collected during FIFE. The method was applied on the 1D subcatchment on the Konza Prairie with promising results. A more detailed presentation of this work will be made elsewhere. The values of Q_0, f, and Λ employed in this work are 0.0012, 4.0, and 3.74, respectively.

Inspection of Table 1 shows that the values of the soil parameters for the individual soils are very similar. For model calibration purposes, catchment average values of $\theta_s = 0.47$, $\theta_r = 0.05$, $B = 0.17$, and $\psi_B = 0.33$ were used

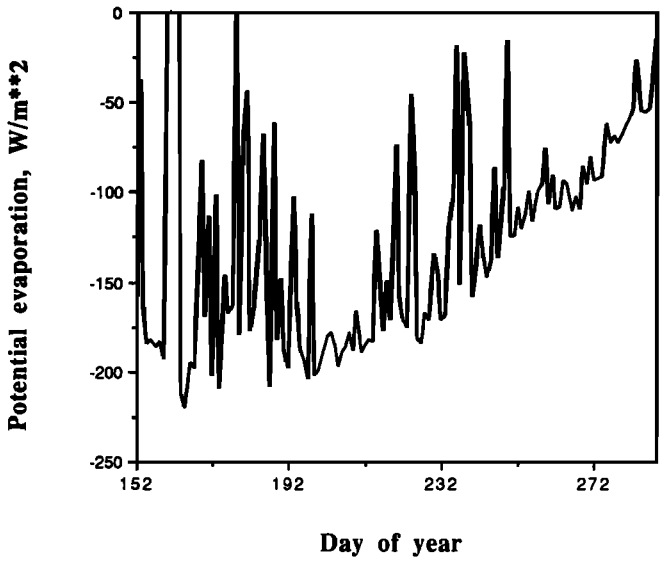

Fig. 4. Computed daily potential evaporation for site 2 (1916-BRS) from June 1 to October 9, 1987.

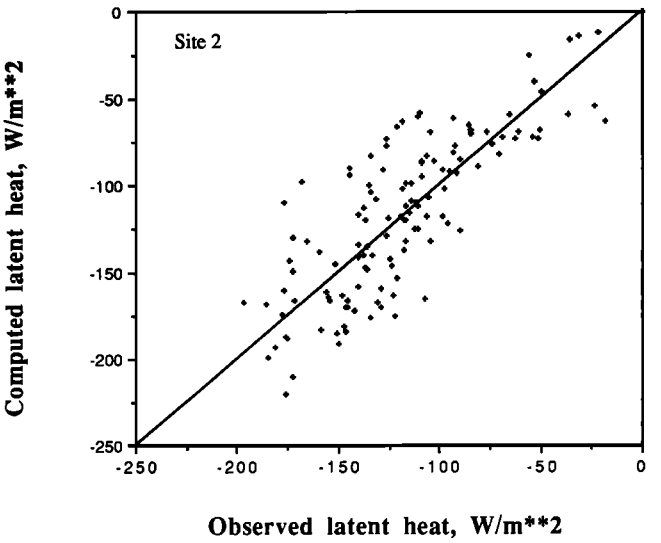

Fig. 6. Computed versus observed latent heat at site 2 (daily) from June 1 to October 9, 1987. The solid line represents 1:1 correspondence.

as initial values. *Paniconi* [1992] estimated these parameters from field data collected for the Benfield-Florence complex, the dominant soil type in the catchment. These estimates agree well with the values presented here, except for ψ_B, for which field data yield a value of 0.6. In calibrating the model therefore, these catchment average parameter values were not varied, except for ψ_B, which was increased incrementally toward an upper limit of 0.6. In fact, a value of $\psi_B = 0.6$ was found to give the best results, which are described below.

Model Operation

A model simulation is initialized by estimating $\bar{z}$, the average water table depth. This is accomplished by inversion of (12), from field data, or with the aid of remotely sensed data during hydrologic recession periods [*Famiglietti and Wood*, 1991*b*]. Using (4), the water table depth is determined for each grid square. During each storm time step, an image of rainfall is used to force the model. The resulting streamflow for each grid square is calculated, and the catchment scale flux of runoff is determined. Note that the routing of generated runoff over hillslopes and along stream channels is not included here but has been treated elsewhere in related work [see *Sivapalan et al.*, 1990]. After a storm event ceases, the infiltrated water is allowed to drain to the water table. The average water table depth is then updated, including the appropriate accounting for subsurface flow during the storm.

During interstorm periods a spatially constant but diurnally varying potential evaporation is used to drive the model. A spatially variable atmospheric forcing can easily be incorporated in the model, as in the storm case. At each time step, the local grid fluxes of latent heat are summed over the catchment, as shown earlier. The average water table depth is updated after each time step by accounting for the losses to evaporation and subsurface drainage.

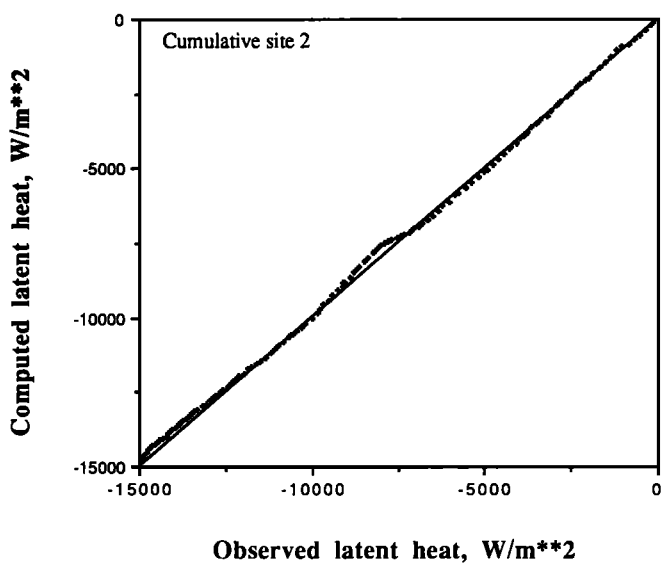

Fig. 5. Computed versus observed latent heat at site 2 (cumulative daily) from June 1 to October 9, 1987. The solid line represents 1:1 correspondence.

RESULTS

The water balance model described in this report was run for the King's Creek catchment for the period from June 1 to October 9, 1987. All model inputs and parameters have been previously described, except the potential evaporation. Daily values of the potential evaporation were computed using the *Priestly and Taylor* [1972] formulation, with α equal to 1.27. Net radiation data from site 2 (1916-BRS), located inside the catchment near its outlet, were used in these calculations. Figure 4 shows the computed daily potential evaporation for this site.

Comparisons are made between the model-computed latent heat and the observations at site 2, between the computed site 2 latent heat and the computed catchment average latent heat, and between the model-computed catchment average latent heat and the latent heat observed at seven sites, including site 2 and six sites reported by *Fritschen and*

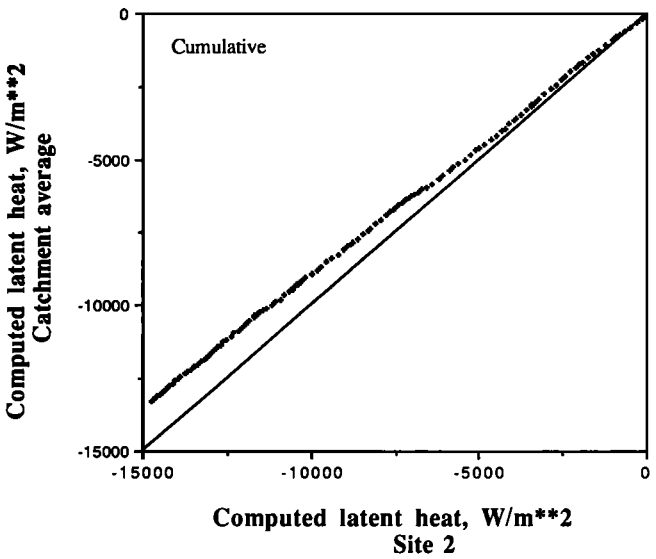

Fig. 7. Computed catchment average latent heat versus computed site 2 latent heat (cumulative daily) from June 1 to October 9, 1987. The solid line represents 1:1 correspondence.

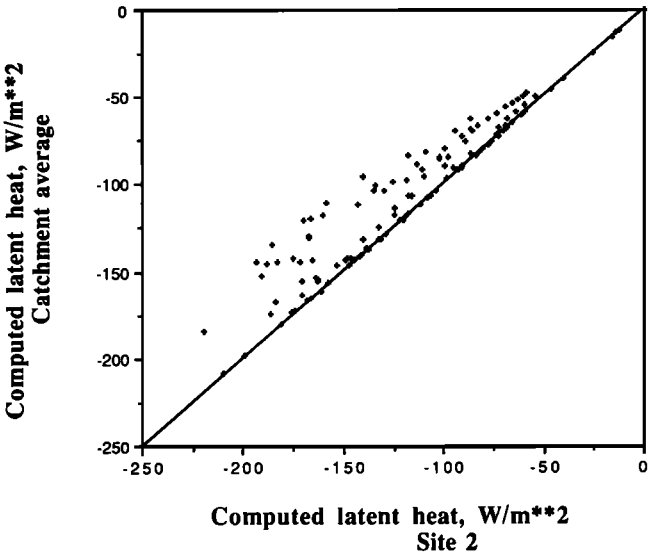

Fig. 8. Computed catchment average latent heat versus computed site 2 latent heat (daily) from June 1 to October 9, 1987. The solid line represents 1:1 correspondence.

Qian [1990]: 20 (6340-BRL), 34 (3479-BRL), 36 (2655-BRL), 40 (1246-BRL), 42 (1445-BRL), and 44 (2043-BRL).

The comparison between the modeled and the observed evaporation at site 2 is shown in Figure 5. The comparison is very good for the period modeled except for the days between July 17 and August 3, when the model predicts slightly lower evaporation than that measured at site 2. Inspection of the precipitation data in Figure 2 shows that this is an extended interstorm period. Modeled evaporation capacities fall exponentially during this period and do not increase until a new storm period begins. This is because the desorptivity is temporally constant for the entire simulation period and thus too low for this particular interstorm period. In a revised model version currently being tested, this term varies in both space and time. Figure 6 provides a scatter plot for the daily computed and observed latent heat fluxes for site 2. Given the simple representation of the evaporation process in the model, the comparison is good.

The comparison between the computed site 2 latent heat and the computed catchment average is given in Figure 7 (for the accumulated values) and Figure 8 (for the daily scatter plot). This comparison shows that the catchment average evaporation is lower than at site 2. This result is intuitively pleasing, since site 2 is situated near the outlet of the catchment, in an area with a high value of the topographic-soil index. These are areas with higher than average soil

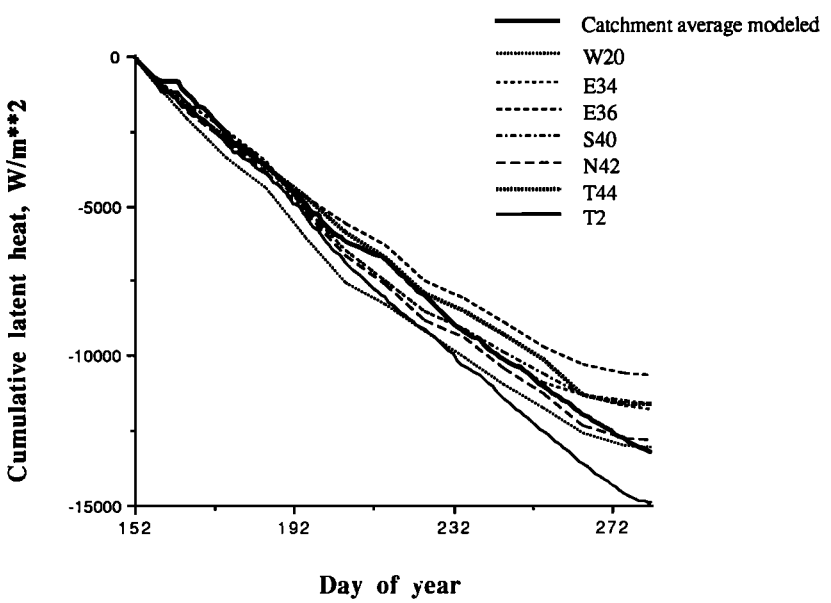

Fig. 9. Computed catchment average latent heat (cumulative daily) and cumulative daily latent heat observed at sites 20, 34, 36, 40, 42, and 44 [*Fritschen and Qian*, 1990] and site 2 from June 1 to October 9, 1987. Letters refer to direction slope faces; T indicates a flat area.

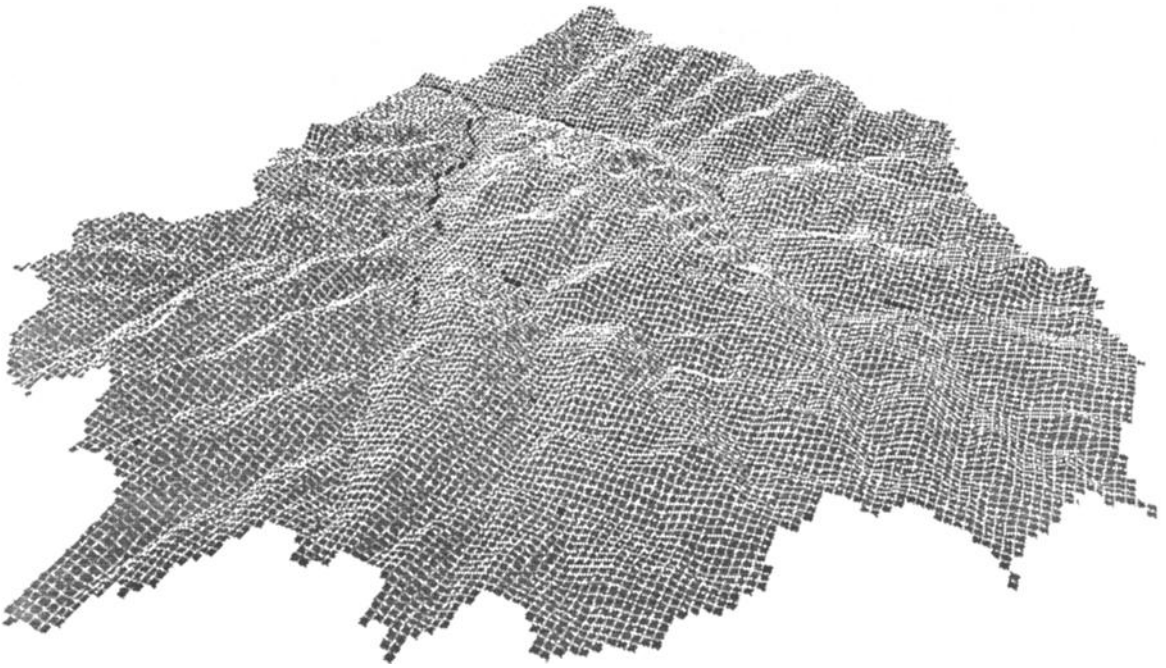

Fig. 10. Modeled evaporation state for King's Creek area of FIFE at 0445 LT, August 13, 1987. Light gray indicates unsaturated areas evaporating at soil-controlled rates; dark gray indicates unsaturated areas evaporating at atmosphere-controlled rates; black indicates saturated areas evaporating at atmosphere-controlled rates.

moisture, resulting in evaporation rates closer to the potential rate.

Comparison of the modeled catchment average latent heat with an observed catchment average is difficult owing to the lack of flux stations within the King's Creek catchment. Figure 9 shows one comparison with six stations reported by *Fritschen and Qian* [1990] and with site 2. The modeled results compare well with observed values. The cumulative catchment average is on the low side of the observed values for the first half of the simulation. This may be caused in part by a sequence of 4 days, beginning on day 160, during which the daily input values of net radiation at site 2 are zero. The calculated potential evaporation is thus zero, which results in a computed evaporative flux of zero for those days. Future work will use the average net radiation from a number of flux stations to drive the interstorm model. During

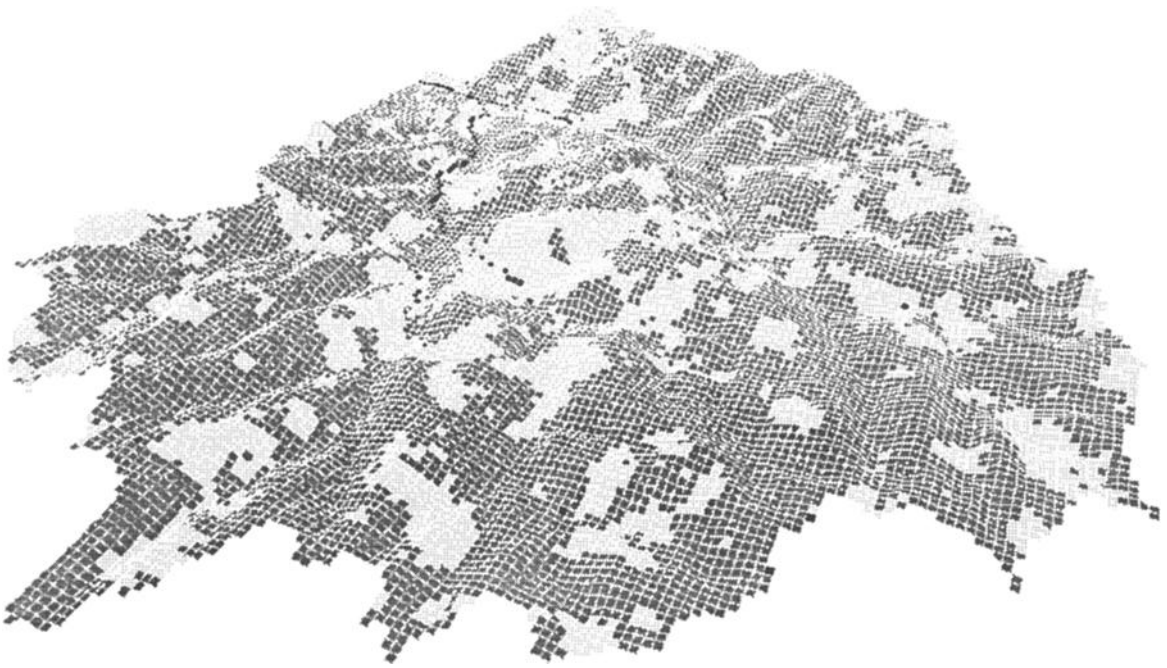

Fig. 11. Modeled evaporation state for King's Creek area of FIFE at 0045 LT, August 15, 1987. Light gray indicates unsaturated areas evaporating at soil-controlled rates; dark gray indicates unsaturated areas evaporating at atmosphere-controlled rates; black indicates saturated areas evaporating at atmosphere-controlled rates.

Fig. 12. Modeled evaporation state for King's Creek area of FIFE at 0245 LT, August 18, 1987. Light gray indicates unsaturated areas evaporating at soil-controlled rates; dark gray indicates unsaturated areas evaporating at atmosphere-controlled rates; black indicates saturated areas evaporating at atmosphere-controlled rates.

the second half of the simulation, the computed catchment average agrees well with the seven-site average.

The ability of the model to differentiate between atmospheric controls and soil controls on evaporation is critical to the modeling of heterogeneous areas. Figures 10 through 12 show the transition of these processes during one particular interstorm period following heavy rainfall on August 12 and 13, 1987. Initially, all of the catchment was evaporating at the potential, or atmosphere-controlled rate. Gradually, more of the evaporative flux was controlled by the ability of the soil column to deliver moisture to the surface. This results in spatially heterogeneous computed evaporation rates, as shown in Figure 13.

SUMMARY

A catchment scale water balance model is presented. The model incorporates spatial variability in topography, soils, and precipitation to predict the land surface hydrologic fluxes. The distributed model presented here represents a first step toward the development of macroscale equations for land surface-atmosphere interactions that preserve sub-

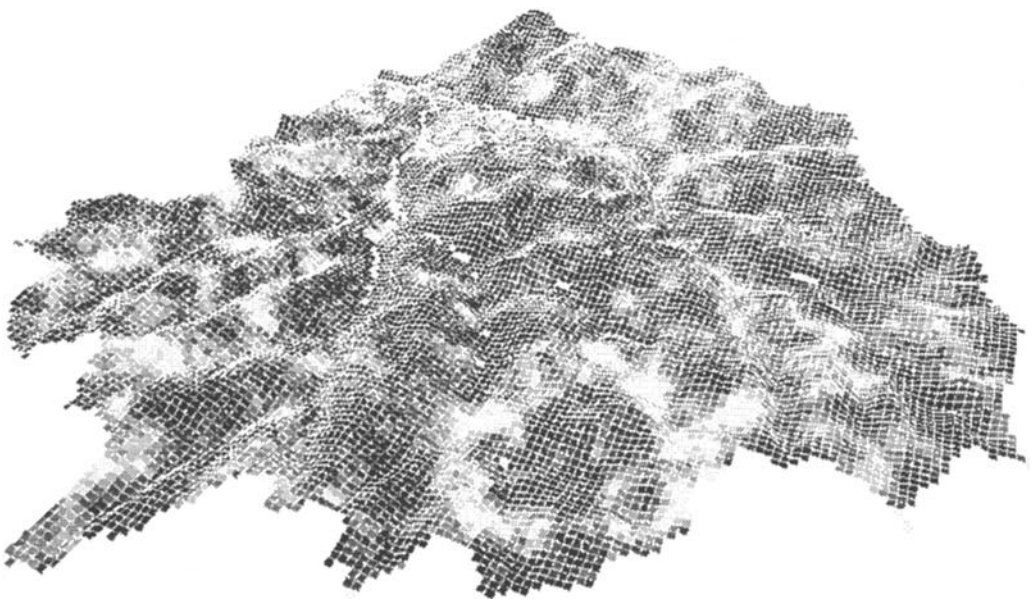

Fig. 13. Modeled evaporation rates for King's Creek area of FIFE at 1330 LT, July 23, 1987. The scale from white to black represents evaporation rates moving from high to low.

grid-scale variability. Comparisons of computed and observed evaporation data show that this approach is promising.

The heterogeneity of the land surface leads to different computed flux rates from different locations in the catchment. The catchment scale fluxes are sums over all locations in the catchment. Verification of these ideas is difficult owing to the lack of flux stations in the King's Creek catchment. However, comparisons of computed and observed evaporation at site 2 and catchment average evaporation to a seven-site average are encouraging.

Current research involves the incorporation of a root zone and an energy balance formulation for evapotranspiration in the model. With the dynamics of land surface-atmosphere interactions then better represented, the model will be verified over a range of observations, including streamflow and soil moisture, as well as evapotranspiration.

Acknowledgments. This work was supported in part by NASA grant NAG-5-899 and NASA Graduate Student Researchers Program grant NGT-60153; this research support is gratefully acknowledged. We thank Eric Smith for providing net radiation and latent heat data at site 2, Roger Beckie for his help with the spatial interpolation of the precipitation data, and L. Venkataraman and Dah-Syang Lin for their help with data retrieval and reduction and figure preparation.

REFERENCES

Beven, K. J., On subsurface stormflow, An analysis of response times, *Hydrol. Sci. J.*, *27*, 505–521, 1982.

Beven, K. J., and M. J. Kirkby, A physically based, variable contributing area model of basin hydrology, *Hydrol. Sci. Bull.*, *24*(1), 43–69, 1979.

Beven, K. J., and E. F. Wood, Catchment geomorphology and the dynamics of runoff contributing areas, *J. Hydrol.*, *65*, 139–158, 1983.

Beven, K. J., M. J. Kirkby, N. Schofield, and A. F. Tagg, Testing a physically-based flood forecasting model (TOPMODEL) for three U. K. catchments, *J. Hydrol.*, *69*, 119–143, 1984.

Brooks, R. H., and A. T. Corey, Hydraulic properties of porous media, *Hydrol. Pap. 3*, Colorado State Univ., Ft. Collins, 1964.

Brutsaert, W., *Evaporation Into the Atmosphere*, 299 pp., D. Reidel, Norwell, Mass., 1982.

Famiglietti, J. S., and E. F. Wood, Evapotranspiration and runoff from large land areas: Land surface hydrology for atmospheric general circulation models, *Surv. Geophys.*, *12*, 179–204, 1991*a*.

Famiglietti, J. S., and E. F. Wood, Comparison of passive microwave and model derived estimates for soil moisture fields, in *Proceedings of the 5th International Colloquium on Physical Measurements and Signatures in Remote Sensing*, European Space Agency, Noordwijk, The Netherlands, 1991*b*.

Fritschen, L. J., and P. Qian, Energy balance components from six sites in a native prairie, in *Symposium on FIFE*, pp. 37–41, American Meteorological Society, Boston, Mass., 1990.

Hillel, D., *Applications of Soil Physics*, 385 pp., Academic, San Diego, Calif., 1980.

Ibrahim, H. A., and W. Brutsaert, Intermittent infiltration into soils with hysteresis, *Proc. Am. Soc. Civ. E, J. Hydraul. Div.*, *94*(HY1), 113–137, 1968.

Jantz, D. R., R. F. Harner, H. T. Rowland, and D. A. Gier, Soil survey of Riley County and part of Geary County, Kansas, 71 pp., U.S. Dept. of Agric., Soil Conserv. Serv. in cooperation with Kansas Agric. Exp. Stn., 1975.

Milly, P. C. D., An event-based simulation model of moisture and energy fluxes at a bare soil surface, *Water Resour. Res.*, *22*(12), 1680–1692, 1986.

Paniconi, C., Hydrologic processes in variably saturated porous media: Analysis of numerical methods for solving the nonlinear Richards equation, and application to catchment scale simulations, Ph.D. thesis, Dep. of Civ. Eng. and Oper. Res., Princeton Univ., Princeton, N. J., 1992.

Philip, J. R., The theory of infiltration, *Soil Sci.*, *83, 84, 85*, 1957.

Priestly, C. H. B., and R. J. Taylor, On the assessment of surface heat flux and evaporation using large scale parameters, *Mon. Weather Rev.*, *100*, 81–92, 1972.

Rawls, W. J., D. L. Brakensiek, and K. E. Saxton, Estimation of soil water properties, *Trans. ASAE*, *25*(5), 1316–1320, 1328, 1982.

Reeves, M., and E. E. Miller, Estimating infiltration for erratic rainfall, *Water Resour. Res.*, *11*(1), 102–110, 1975.

Richards, L. A., Capillary conduction of liquids through porous mediums, *Physics*, *1*, 318–333, 1931.

Sherman, L. K., Comparison of F-curves derived by the methods of Sharp and Holtan and of Sherman and Mayer, *Eos Trans. AGU*, *24*, 465–467, 1943.

Sivapalan, M., and E. F. Wood, A multidimensional model of nonstationary space-time rainfall at the catchment scale, *Water Resour. Res.*, *23*(7), 1289–1299, 1987.

Sivapalan, M., K. Beven, and E. F. Wood, On hydrologic similarity, 2, A scaled model of storm runoff production, *Water Resour. Res.*, *23*(12), 2266–2278, 1987.

Sivapalan, M., E. F. Wood, and K. J. Beven, On hydrologic similarity, 3, A dimensionless flood frequency model using a generalized geomorphologic unit hydrograph and partial area runoff generation, *Water Resour. Res.*, *26*(1), 43–58, 1990.

J. S. Famiglietti, E. F. Wood, and D. J. Thongs, Water Resources Program, Department of Civil Engineering and Operations Research, Princeton University, Princeton, NJ 08544.

M. Sivapalan, Centre for Water Research, The University of Western Australia, Nedlands, Western Australia, 6009.

(Received January 31, 1991;
revised April 23, 1992;
accepted April 28, 1992.)